Thin Solid Films 521 (2012) 239–244

Contents lists available at SciVerse ScienceDirect

Thin Solid Films

journal homepage: www.elsevier.com/locate/tsf

Atomistic simulations of diamond-like carbon growth

Minwoong Joe, Myoung-Woon Moon, Kwang-Ryeol Lee *

Computational Science Center, Korea Institute of Science and Technology, P.O. Box 131, Cheongryang, Seoul 130-650, South Korea

ARTICLE INFO

Available online 2 December 2011

Keywords:
Molecular dynamics
Diamond-like carbon
Amorphous carbon
Subplantation
Thermal spike
Surface roughening

ABSTRACT

Diamond-like carbon (DLC) films are composed of carbon bonds with different hybridizations, including sp^2, sp^3 and even sp^1. Understanding the atomic bonding structure is essential to understanding the properties and optimizing the process parameters of the films. Because of the limited analytical tools for characterizing the atomic bonding structure in amorphous materials, computational research at the atomistic scale could provide significant insight into the structure–property relationships in diamond-like carbon films and has been applied to understanding the various phenomena occurring during DLC film growth. The contributions of the atomistic simulations and electronic structure calculations pertain mainly to three important issues: (i) the sp^3 bond formation and stress generation mechanisms, (ii) the stress reduction mechanism by metal incorporation, and (iii) the impact angle-dependent surface smoothening/roughening mechanisms.

1. Introduction

Diamond-like carbon (DLC), commonly referred to as amorphous carbon (a-C), with a high content of sp^3 bonds, has attracted considerable attention from the scientific community since a thin film of the material was created by Aisenberg and Chabot in 1971 using an ion-beam deposition technique at room temperature [1]. DLC films exhibit properties comparable to those of diamond materials, such as a high mechanical hardness and chemical inertness. These characteristics are attributed to the covalent sp^3 bonding; a high bond strength (7.41 eV for a σ bond in diamond) allows the materials to be both mechanically hard and chemically inert. Such properties are desirable for applications where surface protection is required. With the technical availability of thin DLC film fabrication by various methods, e.g., filtered cathodic vacuum arc and mass-selected ion beam methods, DLC coatings are widely used in industry [2,3].

DLC films with a variety of properties can be generated by tuning the growth conditions, among which the ion energy E has the most critical role. An E in the range of 50–500 eV is usually used for DLC film growth [2]. The dependence of the film structure on the ion energy has been extensively studied by experiments and atomistic simulations, and it is accepted that $E = 50$–100 eV is the optimum energy range for producing a high sp^3 fraction. At relatively low energies, an sp^2-rich film is produced, while at high energies (greater than 100 eV) the sp^3 fraction also begins to decrease [3].

Although DLC films are satisfactory with respect to their superior mechanical properties (hardness = 60–120 GPa), the high residual compressive stress (6–20 GPa) can cause poor adhesion between the film and the substrate [4,5]. Therefore, buckling or even delamination (particularly with hard substrates such as glass) is often encountered [6], which hampers the performance.

Extensive effort has been devoted to understanding the mechanisms that mediate these features of DLC using atomistic simulations such as molecular dynamics (MD). Now, computational methods are becoming more important in shedding light on veiled microscopic details, thanks to the rapid development of both computational power and reliable interatomic potentials (see next section).

In this brief review, we shall focus on two aspects of DLC or hydrogen-free a-C growth: first, what previous MD or ab initio studies have to tell us about (i) the sp^3 bond formation process and the origin of intrinsic high residual compressive stress and (ii) the stress reduction upon the incorporation of a small amount of metal, and second, the origin of surface smoothening or roughening bifurcated by the impact angle.

2. Development of the empirical carbon potential

In this section, a brief history of the empirical carbon potential is introduced. Tersoff developed the general formalism of the empirical potential for a covalent system by considering Si as a representative element [7]. The formalism was soon empirically re-parameterized and applied to carbon systems in 1998 [8]. Although both C and Si are group IV materials and are able to covalently bond with themselves, their amorphous phases display clear differences in bond formation; for a-C, the sp^2 hybridized bonds are contained in the structure, while they appear only as dangling bonds in amorphous silicon (in other words, Si presents an absence of π-bonding) where an sp^3-bonded network is constructed. Thanks to the small differences in the enthalpies of sp^2 and sp^3 lattices, carbon is versatile and is able to form multiple bonds, including single, double and triple

* Corresponding author. Fax: +82 2 958 5509.
E-mail address: krlee@kist.re.kr (K.-R. Lee).

0040-6090/$ – see front matter © 2011 Elsevier B.V. All rights reserved.
doi:10.1016/j.tsf.2011.11.060

bonds, with itself and with other elements, while Si is unable to form multiple bonds due to weak p_π–p_π orbital overlap, the overlap modality involved in forming multiple bonds [9]. A good interatomic potential for carbon should be sensitive to such diverse and unique properties of carbon bonding, thus enabling accurate modeling of the material's chemistry and the related dynamic processes.

Based on the work of Abell [10] and Tersoff, Brenner introduced improved potentials for hydrocarbons in 1990 and 1992 [11,12]. The motivation was to empower atomic-scale dynamics simulations to resolve the issues on diamond films produced by chemical vapor deposition. Although the Abell–Tersoff approach describes C – C bond lengths and energies (including single, double and triple bond) reasonably well, the underlying assumption only takes into account nearest-neighbor interactions and can overestimate the binding energy (so-called "overbinding") for intermediate bonding configurations, e.g., bonding between a three-coordinate C atom (a radical) and a four-coordinate C atom, and favor decidedly unphysical configurations such as a five-coordinate carbon atom, i.e., the overbinding of radicals [13]. In the Brenner potential, such conjugation effects or many-body interactions were taken into account by means of the bond order function [14].

In 2002, Brenner et al. revised the potential to be suitable for extended data sets and called it the 2nd generation reactive empirical bond order (REBO) potential [15]. The REBO potential is capable of modeling chemical interactions, e.g., C – C or C – H covalent bond formation and breaking. To take into account van der Waals interactions between molecules, e.g., forces between graphite layers, the adaptive intermolecular reactive empirical bond order (AIREBO) potential was proposed by Stuart et al. in 2000 [16]. The AIREBO potential includes two additional energy terms besides the REBO energy term for covalent bonding; one is the Lennard–Jones 6–12 potential that represents the attractive van der Waals dispersion interactions for non-bonded long-range intermolecular interactions, and the other is a torsional potential for refining the relative orientations of dihedral angles coupled with single bonds.

Marks introduced the environment-dependent interaction potential (EDIP) for carbon [17]. However, the EDIP is inherently unable to reproduce the correct distances for double and triple C – C bonds [17]. Lee et al. reported the modified embedded atom method (MEAM) interatomic potential for carbon, stating that the MEAM potential is as good as the original Tersoff potential for carbon and is easily extended to various metal–carbon alloy systems [18]. However, thus far, there have been few reports that confirm its capabilities. The reactive force field (ReaxFF) developed by van Duin et al. is the most advanced potential in that it provides a proper way to handle not only the bond order approach but also charge equilibration. Consequently, it can deal with more complex systems and has described many organic and inorganic systems [19,20]. However, MD simulations of DLC film growth with ReaxFF have not yet been reported. Although there are some variants of the potentials described above, this is a functional line-up of the well-recognized empirical carbon potentials. Citation statistics indicate that the Brenner, REBO and AIREBO potentials are still in mainstream use in MD simulations of systems containing C and H [14].

3. The physical origin of the high residual compressive stress of DLC films fabricated by ion-beam methods

There are two widely accepted models used to explain the high residual compressive stress of DLC films: one is the subplantation model, and the other is the thermal spike model. In what follows, computational approaches to address this issue are briefly reviewed. Lifshitz et al. proposed the subplantation model to explain both the high sp^3 fraction and the high compressive residual stress in DLC films generated by energetic ion bombardments [21–23]. Subplantation is a shallow implantation of incident energetic atoms in the subsurface when they have sufficient energy to penetrate the target surface. If deposited at the subsurface, they would induce a local structural distortion of the existing carbon network, producing increased internal stress and densification of the film. Moreover, a tetrahedral sp^3 environment would be more likely to yield at the surface because the surface atoms are less coordinated than the bulk atoms [24–26]. The thermal spike model, however, assumes that a significant fraction of the energy from energetic ions is transferred to the local region near the impacts, causing a 'thermal spike' region or a local melting region. In such a region, carbon atoms would favor a metastable sp^3 site that is made thermodynamically stable under the high pressure and high temperature induced by the thermal spike [26–28].

Uhlmann et al. carried out the first three-dimensional MD simulation with a density-functional-based tight-binding (DFTB) method [29]. For $E > 30$ eV, the effect of subplantation increased substantially due to C incorporation and momentum transfer, while the surface was covered with a defective sp^2-rich structure due to the collision damage. Overall, a composite structure consisting of an sp^2-rich/sp^3-rich layer was developed. For $E < 30$ eV, the incoming C was deposited on the surface, and a rough, sp^2-rich film was generated. This is supportive of the subplantation model rather than the thermal spike model because the atoms in the collision damage region were significantly displaced, and as a result, a low sp^3 fraction and density were obtained.

Kaukonen and Nieminen found through MD simulations with the Tersoff potential that dense diamond-like structures were formed in an energy window of $E = 40$–70 eV, consistent with previous experimental suggestions [30]. This demonstrated that an MD approach using an empirical potential (neglecting electronic processes) is applicable to real deposition processes. The authors argued that the optimal energy window is produced by the interplay between annealing due to local heating and defect generation, both of which are generally attributed to thermal spikes at high energies.

Lee et al. reported MD results supportive of the thermal spike model [31]. The sp^3 fraction reached a peak in an energy window of $E = 50$–75 eV and then decreased at higher energies. The density and the residual stress also exhibited similar trends (Fig. 1). These

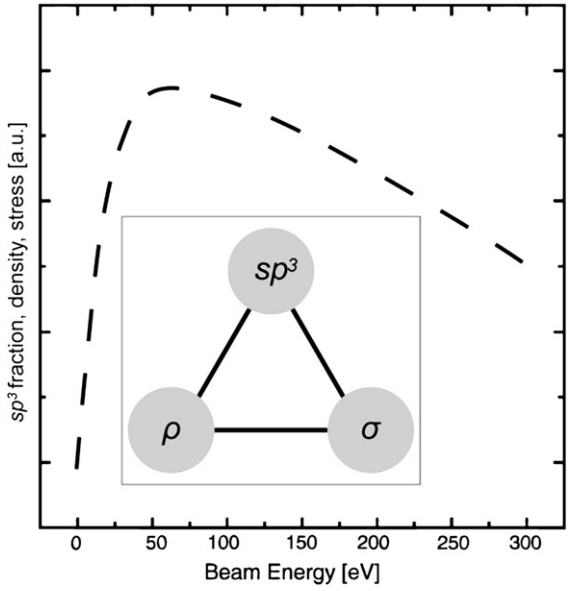

Fig. 1. Nearly identical responses of the three structural factors (the sp^3 fraction, the density ρ, and the stress σ) to the beam energy. Each response curve is collapsed to one curve, which is represented by the dashed line, adapted from Ref [31]. These three components of the DLC are closely coupled with each other; if the sp^3 fraction increases, the density ρ and the stress σ would be increased due to the $\rho \rightarrow \rho_0$ transition and the many distorted bonds involved with the subplantation, respectively (inset).

structural features are strongly coupled with the common structural factor of the three-dimensional interlink, the sp^3 bonding; an increase in the sp^3 fraction by subplantation would lead to many distortions of both the bond angle and the bond length, inducing an increased stress level in the film. Hence, the residual stress, the hardness, and the density of DLC films can have nearly identical dependences on the sp^3 fraction. The link with the thermal spike model could be found in the analysis of the radial distribution function (RDF). The authors found a satellite peak at approximately 2.1 Å in the RDF, which also appeared in Kaukonen's results. This peak was not observed at low energies, but was clearly captured at $E = 50$ eV, which was considered the optimum energy for a high sp^3 fraction in this simulation. Interestingly, this peak was reproduced when molten carbon (at 10,000 K) was rapidly quenched to 0 K at a rate lager than a threshold value. Thus, the satellite peak was attributed to the trapping of carbon atoms in metastable sites. Hard and dense amorphous carbon films, from this point of view, are obtained when the localized thermal spike can be efficiently dissipated to the lattice.

Zhang et al. addressed the stress generation mechanism in DLC films from a different perspective, i.e., the competition between defect generation and defect recovery [32]. They mentioned that one of the drawbacks of the subplantation model [24,26] is its oversimplified picture in which all of the atoms in the subsurface layer are under compressive stress upon the intrusion of incident atoms into the subsurface. The subplantation model can thus be applied to overdense films. However, significant defects such as interstitials and vacancies (the authors regarded a free-volume-shortage and a free-volume-excess as an interstitial and a vacancy in the amorphous structure, respectively) existed in the subsurface layer in their MD simulation. The radiation damage induced by the energetic ion primarily consisted of the creation/annihilation of an interstitial-vacancy pair (Frenkel pair). They calculated the steady-state density of interstitial-vacancy pairs with classical models: the Kinchin and Pease model [33] for the number of displaced atoms and the Seitz and Koehler model (thermal spike model) [27] for the number of recombinations ($E^{5/3}$ scaling). Combined with the elastic theory, such an approximation could give qualitatively good agreement with the film stress behavior under different ion energies; the stress increased linearly at low energies, then peaked at approximately $E = 50$ eV, followed by a power-law decrease at higher energy.

Jäger and Albe obtained a larger sp^3 fraction (close to the value observed experimentally) using the Brenner potential with an increased C–C cutoff [13]. The sp^3 fraction obtained from the Tersoff potential was rather small, that is, less than one half. The authors tried to check whether the original Brenner potential, refined against the overbinding problem of the Tersoff potential, gave a better result for the sp^3 fraction, and surprisingly, a very small value for the sp^3 fraction (resulting in an almost graphitic material) was obtained from the deposition simulations. The main reason for this was identified as the C–C cutoff distance; it was too short to bind with neighboring carbon atoms, and thus by increasing the cutoff distance, structures with realistic densities and sp^3 contents were obtained. The authors claimed that such a high fraction of sp^3 formation was essentially based on a process that occurred in the subsurface. It is also worth noting that the sp^3 fraction critically depends on the substrate temperature as well. After the incorporation of the bombarding ions in the subsurface, relaxation processes leading to the sp^3-to-sp^2 conversion were efficiently suppressed at the time scale of 0.5 ps when the substrate temperature T_s was less than a critical temperature T_c ($\approx$373 K for $E = 40$ eV), while graphitic a-C was formed when $T_s > T_c$ [34].

The MD results above, summarized in Table 1, are equivocal on the subject of which model is superior. Rather, both the subplantation and thermal spike mechanisms may be more or less active, largely depending on the interatomic potential and the simulation method used. This indicates (i) the complexity involved with the ion-surface interaction (that would require a more refined model) and (ii) the limitations of MD modeling associated with the limited accuracy of the empirical potentials and the limited length and time scales (that would require multiscale modeling). Thus, further studies with more accurate potentials and a scale-bridging approach are needed before a consistent conclusion may be drawn.

Table 1
Comparison of the DLC films obtained by MD simulations. The values shown here are for the cases with the highest sp^3 fractions.

Potential	Growth conditions				Film properties			Ref.
	E [eV]	f [$m^{-2}\,s^{-1}$]	Φ	T_s [K]	Stress [GPa]	ρ/ρ_0	sp^3 ratio [%]	
DFTB	80	1×10^{30}	17	0	–	0.86	75	[29]
Tersoff	40	4×10^{30}	320	300	–	0.95	44	[30]
Tersoff	50–75	1×10^{30}	500	300	11	0.8	48	[31]
Tersoff	60	2×10^{28}	900	300	5	0.83	48	[32]
Brenner	40	2×10^{24}	560	100	9*	0.94	82	[13]
Brenner	70	2×10^{24}	5000	293	8*	0.89	65	[34]

ρ_0: 3.5 g cm^{-3} for diamond.
*: 0 K value.

4. The physical origin of stress reduction in Me-DLC

Metal incorporation is a common strategy for reducing high residual compressive stress in DLC films with no significant degradation of the material properties [35–39]. In this section, we discuss the contributions of metal incorporation to the stress reduction in DLC films based on the previous studies of Wang et al. [40,41] and Choi et al. [42,43].

Wang et al. reported unusual stress behavior when W was incorporated in hydrogenated DLC [40]. The 'unusual' behavior indicates that the film stress is initially drastically decreased, then jumps up, then decreases as the W concentration increases. At a W concentration of 2.8 at.%, the residual stress of the DLC film can be as low as half that of the bare DLC, but no significant deterioration of mechanical properties is observed. However, by further increasing the W concentration up to 3.6 at.%, the compressive stress rapidly increased to 85% of the bare films. This was attributed to the phase segregation of the W in the matrix. At a low concentration, the W atoms are well dispersed in structural harmony with the DLC matrix, while at a higher concentration, phase segregation occurs in a narrow W concentration range (thus, the stress increases dramatically), and the nano-sized WC_{1-x} crystallite evolves upon further increasing of the W concentration, thus, decreasing the film stress.

The stress reduction in the well-dissolved phase was explained by the comparison of the total energy between the C–C and C–W bonds as a function of the bond distortion angle. From ab initio calculations, the variation of the total energy (ΔE) against the deviation of the equilibrium bond angle (109.5°) was very small in the case of a W atom located at the center of the tetrahedron, compared with the case of a C atom. This result implies a "pivotal" role of the W atoms in the amorphous carbon matrix by which the distortion of the atomic bond angles can occur without a significant increase in the strain energy.

Choi et al. investigated the stress reduction behavior in metal-incorporated a-C with various transition metals and noble metals using ab initio calculations [42,43]. The total energy change for the tetrahedral bond model was estimated by distorting the bond angles from the equilibrium angle of 109.5° over the range of 90–130° (Fig. 2). The total energy was significantly increased in the case of the pure carbon model, while it was drastically reduced by the replacement of the central C atom with a metal atom. The transition metals known to form metal carbides, such as Ti, Mo, Cr, and W, exhibited low formation energies for the Me–C tetrahedron as well, implying their chemical affinities with carbon. The noble metals

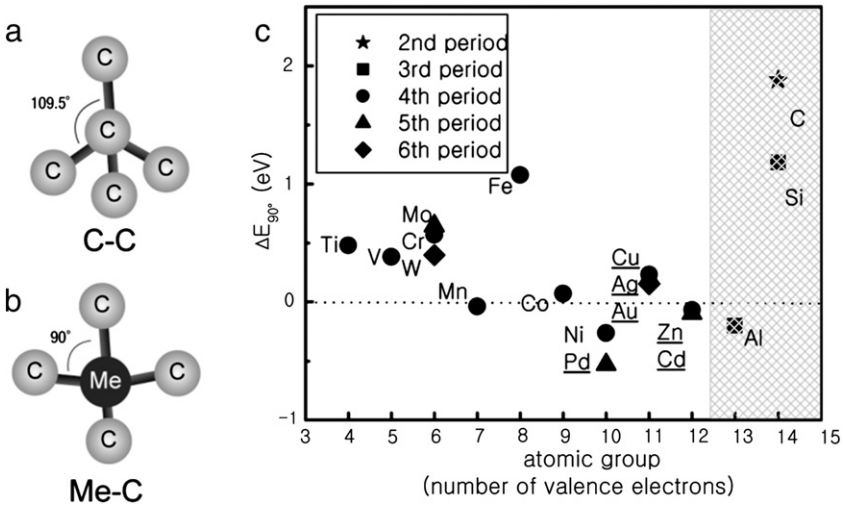

Fig. 2. Schematics of the tetrahedral bond model for C–C (a) and metal–C bonds (b) and the total energy change upon a bond distortion of 90° as a function of the number of valence electrons in the metal atoms (c), Ref. [42].

such as Au and Ag, with fully filled *d*-shells, gave a lower total energy change than the transient metals with partially filled *d*-shells. Thus, the noble metals should be better in reducing the film stress. However, the formation energy for a tetrahedron composed of the noble metals and carbon atoms was approximately two to three times larger than for the transition metals. The Al atom is unique because a negative total energy change was obtained for a bond distortion angle of 90°, implying that Al and C prefer a two-dimensional configuration.

The stress reduction in the metal-incorporated DLC (Me-DLC) can be explained in terms of the characteristics of the bonding between the metal and carbon atoms. From the spatial distribution of electrons involving a bond between a metal and a carbon atom, a more isotropic distribution with a lower density for the metal–carbon bond was typically obtained in contrast with the strong and highly oriented carbon–carbon covalent bond, implying a weak dependence of the bond energy on the bond angle. Thus, the weak and isotropic nature of metal–carbon bonds may contribute to the lower stress level of the Me-DLC film.

In summary, although the tetrahedron bond model reflects only limited configurations of the metal atoms in a carbon network, this model is insightful because the tetrahedrally coordinated (sp^3) bonds are closely related to the changes in the physical and chemical properties of DLC films (as described in Section 3). According to this model, the stress reduction in Me-DLC films is possible without sacrificing hardness due to the pivotal role of metal atoms; a distortion of the atomic bond angle can be present without a significant increase in the elastic energy, which can be viewed as resulting from the weak and less directional Me–C bonds.

5. The physical origin of surface smoothening and roughening according to the angle of incidence

5.1. The smooth surface of DLC under normal incidence

Surface smoothness, sometimes called ultrasmoothness due to an atomic-scale roughness $W<2$ Å, is an intrinsic property of DLC films, typically achieved by the deposition of energetic carbon atoms at normal incidence [44–48]. According to the random deposition model, without a lateral relaxation process, the surface roughness would rapidly increase with power law behavior under prolonged deposition [49]. With this in mind, what is the relevant relaxation process that supports the surface smoothening in DLC film growth? One possibility is thermally activated surface diffusion, which could take into account the surface smoothening as it was derived by Mullins [50,51]. However, the diffusion of covalently bonded carbon atoms is believed to be kinetically unfavorable at room temperature [47,48,52]. Localized melting based on the thermal spike model is possible, but this phenomenon still needs to be proven and remains under debate [46,47,53]. Ballistic diffusion or ion-induced diffusion accompanied by energetic atoms seems plausible. Nearby atoms around an impact site can acquire enough energy to displace transversely on the surface (but not sufficient energy for being sputtered away), and this ion-induced surface diffusion could be the source of smoothening (or roughening). Carter proposed the effect of ballistic atomic drifts parallel to the surface, and derived an incidence-angle dependent smoothening term at the continuum level [54]. Surface smoothening and roughening (or sometimes rippling) of an irradiated Si surface according to the incidence angle was explained by the theory, although the experimental conditions were quite different from those of conventional DLC growth. In line with this, two recent MD results support ion-induced transport as a primary mechanism of smoothening in DLC film growth.

Moseler et al. suggested from multiscale modeling based on the coupling between MD simulations (with both density-functional based tight-binding (DFTB) and the REBO potential) and the continuum equation that the ultrasmoothness of DLC films originates from impact-induced downhill currents at normal or near-normal incidences [47]. The net displacement vector of the surface atoms indicated downhill currents generated when energetic ions bombarded slightly sloped surfaces (0°–20°) under normal incidence, which induced the smoothening of an initially sinusoidal surface after the impact of 4000 C atoms with $E=100$ eV. The impact-induced downhill current $\boldsymbol{j}$ was directly coupled with the local slope $\nabla h(\boldsymbol{x}, t)$ and the ion energy E, and a continuum equation known as the Edwards–Wilkinson equation was constructed with a coefficient obtained from the MD data. This model then gave good agreement with the experimental findings. This shows that such a multiscale modeling approach can realistically simulate the smoothening phenomena occurring during DLC film growth.

Ma et al. reported that the smoothening of an initially rough surface (consisting of hills and valleys) was observed in MD simulations using the REBO potential under normal incidence with $E=20$ eV and 4300 C impacts [55]. The smoothening of the film was mainly attributed to the impact-induced atomic displacements: the authors traced the incident atom and found transverse migration (to a valley) of surface atoms around a hillside, while the movement of the atoms in a valley was restricted, promoting a smooth film.

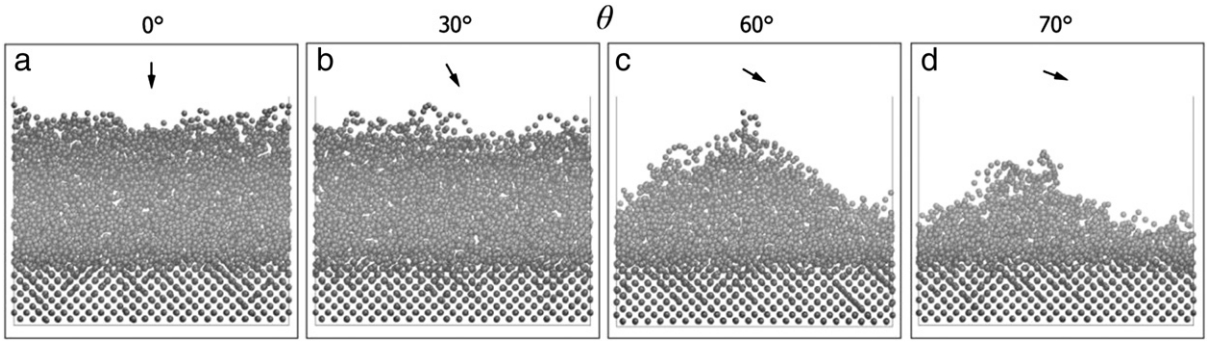

Fig. 3. Cross-sectional snapshots of the growing film after 4000 C impacts with 75-eV kinetic energy under an incidence angle $\theta = 0°$ (a), 30° (b), 60° (c) or 70° (d) (Ref. [56]).

5.2. Rough surfaces produced under grazing incidence angles

As the ion incidence angle becomes grazing, a rough surface is produced. The initial roughening of an a-C film, grown from energetic carbon atoms (40–70 eV), was observed at grazing incidence angles (60°–70°), in sharp contrast with the atomically smooth surface produced under near-normal incidences (0°–30°) [45,48]. Only limited reports are available in which microscopic processes are so far held responsible for the surface roughness evolution of a-C film under grazing incidence [47,55]. The effect of the impact angle, particularly for grazing incidences, has not been clarified yet.

Ma et al. investigated the effect of the incidence angle with a focus on the structural properties of the material, as opposed to the surface roughness. The three structural factors of DLC (i.e., film density, sp^3 fraction, and compressive stress) decreased dramatically as the incidence angle was increased from 0 to 60°. The transverse migration was enhanced by increasing the incidence angle, causing surface relaxation, but the surface roughening was not mentioned.

Joe et al. recently conducted MD simulations with the REBO potential to investigate the initial surface roughening during a-C film growth [56]. Normal or near-normal incidence with an angle of 0° or 30° resulted in a smooth surface for the deposited film. A bump-like surface structure emerged and led to rough surfaces at grazing incidences of 60° or 70° (Fig. 3). These observations are in good agreement with previous experiments. The bifurcated growth mode, depending on the incidence angle, is explained by the net displacement vector of the surface atoms, depending on the local incidence angles. Downhill transport along sloped surfaces, implying smoothening, was dominant at normal incidence, while uphill transport, implying roughening, prevailed at a grazing incidence. This mechanism mediated the initial formation of seed structure and subsequent roughening, driven by shadowing effects under grazing incidence.

6. Conclusions

Atomistic simulations, particularly MD simulations, have been fruitfully applied to finding relevant physical or chemical mechanisms for various phenomena during DLC or a-C film growth. Their contributions, which shed light on three important issues, have been covered in this article: (i) the sp^3 bond formation and stress generation mechanism, (ii) the stress reduction mechanism of metal incorporation, and (iii) the impact angle-dependent surface smoothening/roughening mechanism. Due to their importance in MD simulations, brief history of the empirical potentials for carbon was also given. An obvious future direction in atomistic simulations of DLC growth is the exploration of more reliable interatomic potentials that can correctly capture the sp^3 fraction during the DLC film formation, for which the previous results are rather inconsistent with each another, as discussed in Sections 2 and 3. In particular, further development of a multicomponent potential is needed to allow a detailed understanding of the alloy formation and the stress reduction in Me-DLC film growth, as discussed in Section 4. To better understand the morphological evolution of the DLC surface, as discussed in Section 5, it is helpful to examine self-organized pattern formation under grazing incidence. This is caused by the interplay of the many seed structures that would be expected in a large-scale simulation and still remains challenging.

Acknowledgments

The present work was financially supported by the KIST research program (2E22200) and by the Converging Research Center Program through the Ministry of Education, Science and Technology (2010K000992).

References

[1] S. Aisenberg, R. Chabot, J. Appl. Phys. 42 (1971) 2953.
[2] K.-R. Lee, K. Eun, Bull. Korean Inst. Met. Mater. 6 (1993) 345.
[3] J. Robertson, Mater. Sci. Eng., R: Rep. 37 (2002) 129.
[4] J. Schwan, S. Ulrich, T. Theel, H. Roth, H. Ehrhardt, P. Becker, S.R.P. Silva, J. Appl. Phys. 82 (1997) 6024.
[5] A.C. Ferrari, B. Kleinsorge, N.A. Morrison, A. Hart, V. Stolojan, J. Robertson, J. Appl. Phys. 85 (1999) 7191.
[6] K.-R. Lee, Y. Baik, K. Eun, Diamond Relat. Mater. 2 (1993) 218.
[7] J. Tersoff, Phys. Rev. B 37 (1988) 6991.
[8] J. Tersoff, Phys. Rev. Lett. 61 (1988) 2879.
[9] P. Mélinon, B. Masenelli, F. Tournus, A. Perez, Nat. Mater. 6 (2007) 479.
[10] G. Abell, Phys. Rev. B 31 (1985) 6184.
[11] D.W. Brenner, Phys. Rev. B 42 (1990) 9458.
[12] D.W. Brenner, Phys. Rev. B 46 (1992) 1948.
[13] H. Jäger, K. Albe, J. Appl. Phys. 88 (2000) 1129.
[14] E. Neyts, Mathematical Simulation of the Deposition of Diamond-like Carbon (DLC) Films, Universiteit Antwerpen, 2006.
[15] D.W. Brenner, O.A. Shenderova, J.A. Harrison, S.J. Stuart, B. Ni, S.B. Sinnott, J. Phys. Condens. Matter 14 (2002) 783.
[16] S.J. Stuart, A.B. Tutein, J.A. Harrison, J. Chem. Phys. 112 (2000) 6472.
[17] N. Marks, Phys. Rev. B 63 (2000) 1.
[18] B. Lee, J. Lee, Calphad 29 (2005) 7.
[19] A.C.T. van Duin, S. Dasgupta, F. Lorant, W.A. Goddard, J. Phys. Chem. A 105 (2001) 9396.
[20] S.R. Phillpot, S.B. Sinnott, Science 325 (2009) 1634.
[21] Y. Lifshitz, S. Kasi, J. Rabalais, Phys. Rev. Lett. 62 (1989) 1290.
[22] Y. Lifshitz, S. Kasi, J. Rabalais, W. Eckstein, Phys. Rev. B 41 (1990) 10468.
[23] Y. Lifshitz, Diamond Relat. Mater. 8 (1999) 1659.
[24] J. Robertson, Diamond Relat. Mater. 2 (1993) 984.
[25] J. Robertson, Diamond Relat. Mater. 3 (1994) 361.
[26] C. Davis, Thin Solid Films 226 (1993) 30.
[27] F. Seitz, J.S. Koehler, Solid State Phys. 2 (1956) 305.
[28] D. McKenzie, D. Muller, B. Pailthorpe, Phys. Rev. Lett. 67 (1991) 773.
[29] S. Uhlmann, T. Frauenheim, Y. Lifshitz, Phys. Rev. Lett. 81 (1998) 641.
[30] M. Kaukonen, R. Nieminen, Phys. Rev. B 61 (2000) 2806.
[31] S.-H. Lee, C.-S. Lee, S.-C. Lee, K.-H. Lee, K.-R. Lee, Surf. Coat. 177–178 (2004) 812.
[32] S. Zhang, Acta Mater. 51 (2003) 5211.
[33] G. Kinchin, R. Pease, Rep. Prog. Phys. 18 (1955) 1.
[34] H. Jäger, A. Belov, Phys. Rev. B 68 (2003) 1.
[35] X. Fan, E. Dickey, S. Pennycook, M. Sunkara, Appl. Phys. Lett. 75 (1999) 2740.
[36] A.A. Voevodin, J.P. O'Neill, S.V. Prasad, J.S. Zabinski, J. Vac. Sci. Technol., A: Vac. Surf. Films 17 (1999) 986.
[37] P. Zhang, B.K. Tay, C.Q. Sun, S.P. Lau, J. Vac. Sci. Technol., A: Vac. Surf. Films 20 (2002) 1390.

[38] B. Shi, W. Meng, L. Rehn, P. Baldo, Appl. Phys. Lett. 81 (2002) 352.
[39] C. Corbella, Surf. Coat. Technol. 177–178 (2004) 409.
[40] A.-Y. Wang, H.-S. Ahn, K.-R. Lee, J.-P. Ahn, Appl. Phys. Lett. 86 (2005) 111902.
[41] A.-Y. Wang, K.-R. Lee, J.-P. Ahn, J.H. Han, Carbon 44 (2006) 1826.
[42] J.-H. Choi, H.-S. Ahn, S.-C. Lee, K.-R. Lee, J. Phys. Conf. Ser. 29 (2006) 155.
[43] J.-H. Choi, S.-C. Lee, K.-R. Lee, Carbon 46 (2008) 185.
[44] X. Shi, L. Cheah, J. Shi, Z. Sun, B. Tay, J. Phys. Condens. Matter 11 (1999) 185.
[45] D. Liu, G. Benstetter, E. Lodermeier, J. Vancea, J. Vac. Sci. Technol., A: Vac. Surf. Films 21 (2003) 1665.
[46] C. Casiraghi, A. Ferrari, J. Robertson, Diamond Relat. Mater. 14 (2005) 913.
[47] M. Moseler, P. Gumbsch, C. Casiraghi, A.C. Ferrari, J. Robertson, Science 309 (2005) 1545.
[48] Y. Lifshitz, R. Edrei, A. Hoffman, E. Grossman, G. Lempert, J. Berthold, B. Schultrich, H. Jäger, Diamond Relat. Mater. 16 (2007) 1771.
[49] A.-L. Barabási, H.E. Stanley, Fractal Concepts in Surface Growth, Cambridge University Press, Cambridge, 1995.
[50] W.W. Mullins, J. Appl. Phys. 28 (1957) 333.
[51] W.W. Mullins, J. Appl. Phys. 30 (1959) 77.
[52] Q. Wei, Z.Y. Pan, Z.J. Li, Z.X. Zhang, L.K. Zang, Y.X. Wang, X.S. Ye, T. Bai, C. Wang, J.R. Liu, Phys. Rev. B 68 (2003) 235408.
[53] C. Casiraghi, A. Ferrari, R. Ohr, A. Flewitt, D. Chu, J. Robertson, Phys. Rev. Lett. 91 (2003) 1.
[54] G. Carter, V. Vishnyakov, Phys. Rev. B: Condens. Matter 54 (1996) 17647.
[55] T. Ma, Y. Hu, H. Wang, X. Li, J. Appl. Phys. 101 (2007) 014901.
[56] M. Joe, M.-W. Moon, J. Oh, K.-H. Lee, K.-R. Lee, Carbon 50 (2012) 404.